



Selective oxidation of 1,2-propanediol to lactic acid catalyzed by nanosized Mg(OH)₂-supported bimetallic Au–Pd catalysts



Yonghai Feng^{a,b}, Hengbo Yin^{a,*}, Aili Wang^a, Dezhi Gao^a, Xiaoyan Zhu^a, Lingqin Shen^a, Minjia Meng^a

^a Faculty of Chemistry and Chemical Engineering, Jiangsu University, Zhenjiang 212013, China

^b School of Material Science and Engineering, Jiangsu University, Zhenjiang 212013, China

ARTICLE INFO

Article history:

Received 15 March 2014

Received in revised form 19 May 2014

Accepted 20 May 2014

Available online 28 May 2014

Keywords:

1,2-Propanediol

Bimetallic Au–Pd nanoparticles

Mg(OH)₂ nanoslices

Selective oxidation

Lactic acid

ABSTRACT

1,2-Propanediol co-produced in the dimethyl carbonate production is oversupplied in market. 1,2-Propanediol can also be facilely produced starting from glycerol, which is oversupplied in the biodiesel production. Catalytic conversion of low-valued 1,2-propanediol to high-valued and environmental benign lactic acid was investigated under mild reaction conditions over Au–Pd/Mg(OH)₂ catalysts in our present work. The Au–Pd/Mg(OH)₂ catalysts were prepared by the sol-immobilization method and characterized by XRD, SEM, HRTEM, UV-vis DRS, and O₂-TPD techniques. Small-sized Au and Pd nanoparticles were coalesced together to form secondary nanoparticles, which were well dispersed on the surfaces of Mg(OH)₂ nanoslices. The Au and Pd nanoparticles synergistically catalyzed the oxidation of 1,2-propanediol with O₂ to lactic acid in an alkaline solution. When the catalytic oxidation of 1,2-propanediol was carried out over Au_{0.75}Pd_{0.25}/Mg(OH)₂ catalyst at 60 °C for 240 min, the lactic acid selectivity of 88% was obtained at the 1,2-propanediol conversion of 97.5%. A power-function type reaction kinetic model well fitted the experimental data, $r = -dC_P/dt = kC_P^{0.8}P_{O_2}^{1.4}W_{cat}^{1.0}$. The reaction activation energy was 64 kJ mol⁻¹.

© 2014 Elsevier B.V. All rights reserved.

1. Introduction

Conventional resources, mainly fossil fuels, are becoming limited for the rapid increase in energy demand. Biomass is one of renewable resources and can be used to produce various chemicals and fuels. Using renewable biomass for the synthesis of chemicals is greatly highlighted in chemical research field [1].

Recently, glycerol has been used as an important and renewable feedstock for the synthesis of valuable chemicals via hydrogenolysis [2,3], oxidation [4–6], dehydration [7,8], esterification [9], transesterification [10] processes because large amount of glycerol is produced as a by-product with a yield of ca. 10% in biodiesel production [11,12]. From among the above mentioned processes, hydrogenolysis of glycerol to 1,2-propanediol with the yield of more than 90% is more facilely achieved than to 1,3-propanediol with the yield of less than 27% [1,2]. However, 1,2-propanediol is also facing the oversupply problem because it is produced in a large scale with the scaling-up co-production of dimethyl carbonate and

1,2-propanediol by the transesterification method. 1,2-Propanediol is, at present, mostly used as an organic solvent and a starting material of unsaturated polyester resin, limiting its application. Therefore, effective conversion of the oversupplied 1,2-propanediol to high valuable chemicals is worthy of investigation, considering the profitability of biodiesel and dimethyl carbonate production for environmental protection.

Lactic acid is conventionally used as an acidulant and a preservative in food industry. Recently, lactic acid has been used as a raw material for the production of pharmaceutical, cosmetic, textile, leather, and biodegradable polylactide [13,14]. Polylactide has widespread applications in a variety of fields because it is biodegradable, biocompatible, and applicable [15]. In light of the consumption of polylactide, lactic acid becomes an important chemical with ca. 120 kt annum⁻¹ worldwide production [16]. Lactic acid can be manufactured either by chemical synthesis or by carbohydrate fermentation. However, the latter, predominating the lactic acid production, has several disadvantages, such as large amount of water spending, low reaction rate, and high cost due to its downstream separation and purification [16]. Biological sludge is also unavoidably produced. Therefore, developing environmental benign and low cost chemical synthesis route of lactic acid has attracted researchers' great interest.

* Corresponding author. Tel.: +86 0 511 88787591; fax: +86 0 511 88791800.

E-mail address: yin@ujs.edu.cn (H. Yin).

Nomenclature

A	pre-exponential factor
C_p	initial 1,2-propanediol concentration (mol L^{-1})
E_a	activation energy (kJ mol^{-1})
k	rate constant
r	oxidation rate ($\text{mol L}^{-1} \text{s}^{-1}$)
P_{O_2}	O_2 pressure (MPa)
R	gas constant ($8.314 \times 10^{-3} \text{ kJ mol K}^{-1}$)
T	temperature (K)
W_{cat}	catalyst loading (g)

Conventionally, lactic acid can be produced by the reaction of acetaldehyde with HCN followed by the hydrolysis with sulfuric acid [17]. As compared with the fermentation process, this chemical route has high reaction rate. However, high toxic HCN is used. Recently, several groups have investigated the synthesis of lactic acid from glycerol. Ochoa-Gómez et al. [18] reported that hydrothermal reaction of glycerol with NaOH at 300 °C could produce lactic acid with high yield. The formation of lactic acid from glycerol can also be carried out in an alkaline solution at 200 °C under 0.6 MPa of H_2 [19]. Heeres et al. [20] reported that the maximum lactic acid yield of 80% was obtained when bimetallic Au-Pt/CeO₂ was used as the catalyst under 0.5 MPa of O_2 at 100 °C with the mole ratio of NaOH to glycerol 4:1. These previous studies revealed that the synthesis of lactic acid from glycerol should be carried out at high temperature and pressure in an alkaline surrounding.

Owing to that 1,2-propanediol can be easily produced by the hydrogenolysis of glycerol and the co-production of dimethyl carbonate and 1,2-propanediol, 1,2-propanediol becomes a favorable starting material for the production of lactic acid by catalytic oxidation [17,21–25], fermentation [26], and electro-catalytic oxidation [27]. From among the above mentioned routes, catalytic oxidation of 1,2-propanediol to lactic acid is a more efficient and environmentally friendly route, giving high yield of lactic acid under mild reaction conditions [17,21–25].

It has been reported that supported monometallic and bimetallic Au, Pd, and Pt catalysts are effective for the oxidation of 1,2-propanediol to lactic acid in alkaline medium [17,22–25]. Tsujino et al. [25] firstly reported that Pd/C catalysts modified with Pb, Bi, and/or Te could oxidize 1,2-propanediol to lactic acid, hydroxyacetone, and pyruvic acid. Pinxt et al. [24] reported that Pt/graphite catalysts modified with Pb, Bi, and Sn showed unsatisfactorily catalytic activity in the oxidation of 1,2-propanediol to lactic acid. Although the supported Pd and Pt catalysts give low selectivity of lactic acid, these pioneer studies reveal that 1,2-propanediol can be converted to lactic acid by catalytic oxidation.

Hutchings et al. [28] found that supported Au catalyst showed high catalytic activity in the oxidation of 1,2-propanediol to lactic acid at 60 °C, giving the lactic acid selectivity of 71% at the 1,2-propanediol conversion of 53%. Then, they studied the oxidation of 1,2-propanediol over carbon-supported Au-Pd [17], Au-Pt [22,23], and Pd-Pt [22,23] catalysts. As compared with Au-Pd/C and Pd-Pt/C catalysts, Au-Pt/C catalyst showed high catalytic activity for the conversion of 1,2-propanediol to lactic acid, giving the lactic acid selectivity of 96% at the 1,2-propanediol conversion of 95% [23]. Xu et al. [21] investigated the effect of support types on the conversion of 1,2-propanediol to lactic acid. It was found that Au/MgO gave the lactic acid selectivity of 89.3% at the 1,2-propanediol conversion of 94.4% when the reaction was carried out under 0.3 MPa of O_2 at 60 °C for 6 h. Au/MgO catalyst showed higher catalytic activity in the catalytic oxidation reaction than the Au/graphite and Au/TiO₂ catalysts [17,28]. The previous works

reveal that noble metals are potentially active components in the catalytic oxidation of 1,2-propanediol to lactic acid. The property of support also affects the catalytic activity. However, the effect of the physicochemical properties of supported Au-based catalysts on the oxidation of 1,2-propanediol to lactic acid has not been systematically investigated.

In our present work, nanosized Mg(OH)₂-supported Au, Pd, and Au-Pd catalysts were prepared by the sol-immobilization method and used in the catalytic oxidation of 1,2-propanediol to lactic acid under mild reaction conditions. The as-prepared Mg(OH)₂-supported Au-based catalysts were characterized by XRD, HRTEM, O₂-TPD, and UV-vis DRS techniques. The Au-Pd/Mg(OH)₂ catalysts showed high catalytic activities in the liquid phase oxidation of 1,2-propanediol with molecular oxygen to lactic acid. A power-function type reaction kinetic model was used to evaluate the effect of reaction parameters. The reaction mechanism for the oxidation of 1,2-propanediol to lactic acid was briefly discussed.

2. Experimental

2.1. Materials

The chemicals, magnesium chloride ($\text{MgCl}_2 \cdot 6\text{H}_2\text{O}$), sodium hydroxide (NaOH), sodium borohydride (NaBH_4), chloroauric acid ($\text{HAuCl}_4 \cdot 3\text{H}_2\text{O}$), palladium chloride (PdCl_2), magnesium hydroxide (Mg(OH)_2), polyvinyl alcohol, 1,2-propanediol, lactic acid, formic acid, acetic acid, and hydroxyacetone were of reagent grade and were purchased from Sinopharm Chemical Reagent Co., Ltd. China. Acetonitrile was of chromatographic grade and was purchased from Sinopharm Chemical Reagent Co., Ltd. China. All chemicals were used as received without further purification.

2.2. Preparation of catalysts

Nanosized Mg(OH)₂ slices were prepared by the coprecipitation method using magnesium chloride hexahydrate as the precursor and sodium hydroxide as the precipitating agent. 500 mL of NaOH (4 mol L⁻¹) aqueous solution was dropwise added into 200 mL of MgCl_2 (2.5 mol L⁻¹) aqueous solution under mild stirring at room temperature. The suspension was aged for 4 h and then filtrated and washed with distilled water until the pH value of filtrate was close to 7. Then, the washed Mg(OH)₂ was dried at 120 °C overnight. The as-prepared Mg(OH)₂ had a specific surface area of 69.5 m² g⁻¹, a pore volume of 0.67 cm³ g⁻¹, and an average pore diameter of 4.3 nm, which were measured by the N₂ adsorption/desorption method and calculated by the BET and BJH methods, respectively.

$\text{Au}_x\text{Pd}_y/\text{Mg(OH)}_2$ catalysts (x and y , weight ratios of Au and Pd to $\text{Mg(OH)}_2 \times 100$) were prepared by the sol-immobilization method. Firstly given amounts of PdCl_2 and $\text{HAuCl}_4 \cdot 3\text{H}_2\text{O}$ were dissolved in 7 mL of polyvinyl alcohol (1%) aqueous solution. Then, 7 mL of freshly prepared NaBH_4 (0.1 mol L⁻¹) aqueous solution was added into the above solution to produce a dark-brown sol. After aging at room temperature for 30 min, the reduced metallic Au and Pd colloids were immobilized by adding 5 g of nanosized Mg(OH)₂ slices under vigorous stirring for 2 h. The as-prepared Au-Pd/Mg(OH)₂ catalysts were filtrated, washed with distilled water, and dried at 120 °C overnight. The compositions of the Au-Pd/Mg(OH)₂ catalysts are listed in Table 1. The inductively coupled plasma (ICP) analysis showed that the contents of Au and Pd in Au-Pd/Mg(OH)₂ catalysts were similar to those calculated according to their precursors, indicating that Au and Pd were effectively supported on the surfaces of nanosized Mg(OH)₂ slices by the sol-immobilization method.

Table 1
Physicochemical properties and catalytic activities of Au–Pd/Mg(OH)₂ catalysts.

Catalysts	Specific surface areas (m ² g ⁻¹)	Amounts of Au and Pd ^a (μmol g ⁻¹)		Average particle sizes of Au and Pd ^b (nm)		Total O ₂ adsorption amounts (μmol g ⁻¹)	O ₂ amounts adsorbed on both Au and Pd nanoparticles ^c (μmol g ⁻¹)	Conversions of 1,2-propanediol (%)	Selectivities (%)	TOF ^e (h ⁻¹)
		Au	Pd	Au	Pd					
Au ₁ /Mg(OH) ₂	68.2	53.4	0	6	—	110	19.5	30.5	7.8	1019
Al _{0.75} Pd _{0.25} /Mg(OH) ₂	64.3	38.5	22.8	5	2	114.9	24.4	60.9	3.8	94.0
Al _{0.5} Pd _{0.5} /Mg(OH) ₂	68.6	25.1	44.7	4	4	108.4	17.9	48.9	3.0	95.3
Al _{0.25} Pd _{0.75} /Mg(OH) ₂	65.1	12.4	68.3	3	5	108.6	18.1	37.4	2.1	96.6
Pd ₁ /Mg(OH) ₂	64.2	0	90.9	—	4	109.1	18.6	18.3	2.6	92.6
Au _{1.5} Pd _{0.5} /Mg(OH) ₂	63.7	76.4	46.3	5	2	130.5	40	95.4	8.0	83.8
Mg(OH) ₂	69.5	—	—	—	—	90.5	—	0	—	8.2
Al _{0.75} Pd _{0.25} /bulk-Mg(OH) ₂ ^f	8.3	31.5	18.8	—	—	38.9	8.3	10.2	14.3	63.4
Bulk Mg(OH) ₂	9.9	—	—	—	—	30.6	—	0	—	22.3

^a The amounts of Au and Pd supported on Mg(OH)₂ nanoparticles were analyzed by ICP.

^b The average particle sizes of Au and Pd were calculated according to HRTEM images.

^c O₂ amounts adsorbed on both Au and Pd nanoparticles = total O₂ adsorption amounts – O₂ amounts adsorbed on support.

^d Reaction conditions: stirring rate, 700 rpm; reaction temperature, 60 °C; weight of catalyst, 0.4 g; NaOH concentration, 0.52 mol L⁻¹; 1,2-propanediol solution, 0.26 mol L⁻¹, 200 mL; O₂ pressure, 1.0 MPa, reaction time, 1 h.

^e TOF (h⁻¹) = reacted 1,2-propanediol (mol) in 1 h divided by the amount of atomic O (mole) adsorbed on both Au and Pd nanoparticles of catalyst.

^f Au and Pd supported on bulk Mg(OH)₂ particles.

To compare the effect of supports on the 1,2-propanediol oxidation reaction, Au–Pd/bulk-Mg(OH)₂ was also prepared according to the method described above. Commercial bulk Mg(OH)₂ powders were used as supports instead of Mg(OH)₂ nanoslices.

2.3. Characterization

The X-ray powder diffraction (XRD) spectra of the Mg(OH)₂ and Au–Pd/Mg(OH)₂ catalysts were recorded on a diffractometer (D8 super speed Bruke-AEX Company, Germany) using Cu K α radiation ($\lambda = 1.54056 \text{ \AA}$) with Ni filter, scanning from 10° to 90° (2θ).

Scanning electron microscopy (SEM) was performed on a scanning electron microscope (JSM 7001F) operated at an acceleration voltage of 10 kV to characterize the morphology of Mg(OH)₂ particles. High resolution transmission electron microscopy (HRTEM) images were obtained on a microscope (JEM-2100) operated at an acceleration voltage of 200 kV to characterize the morphologies and the crystal structures of the Au and Pd nanoparticles supported on Mg(OH)₂ nanoslices. The TEM specimens were prepared by placing a drop of Au–Pd/Mg(OH)₂ ethanol suspension onto a copper grid coated with a layer of amorphous carbon. The average particle sizes of the Au and Pd nanoparticles were measured from the TEM and HRTEM images. The average particle sizes of the Au and Pd nanoparticles were calculated by a weighted-average method according to the individual particle sizes of the all counted particles.

Temperature-programmed desorption of O₂ (O₂-TPD) was carried out in a fixed-bed continuous flow microreactor at atmospheric pressure. The samples (0.25 g) were dried at 450 °C for 2 h and then were O₂-saturated in an O₂ stream at 60 °C for 1 h. After purging with helium (30 mL min⁻¹) at 60 °C for 0.5 h to remove the physically adsorbed O₂, the samples were heated at a linear heating rate of 15 °C min⁻¹ up to 700 °C. In order to determine the amounts of adsorbed O₂ from O₂ desorption profiles, the areas under the curves were integrated by the Gaussian deconvolution and the amounts of adsorbed O₂ were expressed as micromoles of O₂ per gram of catalyst.

UV-vis diffuse reflectance spectra of the catalysts were recorded on a UV-2550 spectrophotometer (Shimadzu Co., Kyoto, Japan) equipped with a diffuse reflectance attachment over a wavelength range from 190 to 900 nm. BaSO₄ powder was used as the reference.

The Au and Pd contents of the catalysts were analyzed using inductively coupled plasma (ICP) technique (VISTA-MPX).

The specific surface areas of the catalysts were measured on a NOVA 2000e physical adsorption apparatus and calculated by the BET method.

2.4. Catalytic test

Catalytic oxidation of 1,2-propanediol was carried out in a 1000 mL capacity stainless steel autoclave equipped with a magnetically driven impeller. The autoclave was charged with appointed amounts of 1,2-propanediol, water, sodium hydroxide, and catalyst. First, the autoclave was purged with O₂ for 10 min. Then the pressure was raised to the desired value. Under stirring, the reaction was carried out at given temperature for a certain time. After reaction, the autoclave was cooled to ambient temperature and depressurized.

Before product analysis, the reaction mixture was acidified with hydrochloric acid (12 M) to the pH value of ca. 3. The concentration of remained 1,2-propanediol was analyzed on a gas phase chromatograph equipped with a PEG-20 M packed capillary column (0.25 mm × 30 m) and FID by the internal standard method with n-butanol as the internal standard. The products, such as lactic acid, acetic acid, and formic acid, were analyzed on a Varian HPLC system equipped with a reverse-phase column (Chromspher 5 C18, 4.6 mm × 250 mm) and a UV detector ($\lambda = 210 \text{ nm}$) at 35 °C. The

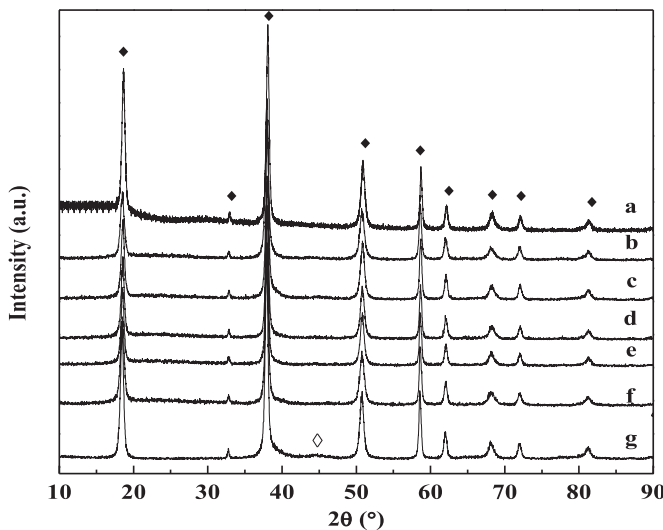


Fig. 1. XRD patterns of (a) Mg(OH)₂, (b) Au₁/Mg(OH)₂, (c) Au_{0.75}Pd_{0.25}/Mg(OH)₂, (d) Au_{0.5}Pd_{0.5}/Mg(OH)₂, (e) Au_{0.25}Pd_{0.75}/Mg(OH)₂, (f) Pd₁/Mg(OH)₂, and (g) Au_{1.5}Pd_{0.5}/Mg(OH)₂. ♦, Mg(OH)₂; ◇, Au.

mobile phase was composed of H₃PO₄/NaH₂PO₄ (0.1 M NaH₂PO₄ acidified by H₃PO₄ to pH = 2) buffer aqueous solution and acetonitrile (v:v = 9:1) with a flow rate of 0.6 mL min⁻¹. The concentrations of the products were analyzed by the external standard method.

3. Results and discussion

3.1. XRD analysis

Fig. 1 shows the X-ray diffraction patterns of Mg(OH)₂ and Au-Pd/Mg(OH)₂ catalysts. The XRD peaks at $2\theta = 18.59$, 32.84, 38.02, 50.85, 58.64, 62.07, 68.25, 72.03, and 81.25° ascribed to Mg(OH)₂ phase (PDF 07-0239) were observed for all the samples. There were no other magnesium oxides detected by the XRD analysis, indicating that the as-prepared support was phase pure Mg(OH)₂. At high Au loading, the XRD patterns of Au_{1.5}Pd_{0.5}/Mg(OH)₂ catalyst show a weak peak appearing at 44.38°, which was ascribed to that of metallic Au (PDF 04-0784). For the other samples, there were no XRD peaks of metallic Au and Pd detected, indicating that metallic Au and Pd nanoparticles were well dispersed on the surfaces of support Mg(OH)₂. It can be explained as being due to that when Mg(OH)₂ particles were mixed with noble metallic sol, the surfaces of Mg(OH)₂ particles were positively charged because the pH value of sol was ca. 8, lower than the isoelectric point (IEP) of Mg(OH)₂ (12.2 ± 0.2) [21]. The negatively charged Au or Pd sol could be rapidly adsorbed on the positively charged surfaces of Mg(OH)₂ particles to form well-dispersed nanoparticles.

3.2. SEM and TEM analysis

The SEM images of the as-prepared and bulk Mg(OH)₂ samples are shown in **Fig. 2**. The as-prepared Mg(OH)₂ powders were irregular slices with the average diameter and the average thickness of ca. 60 and 5 nm, respectively. The commercial bulk Mg(OH)₂ powders were polygonal slices with the average diameter and the average thickness of ca. 520 and 60 nm. As compared with bulk Mg(OH)₂, small-sized Mg(OH)₂ nanoslices were prepared under our present experimental conditions.

The TEM and HRTEM images of the Au/Mg(OH)₂, Au-Pd/Mg(OH)₂, and Pd/Mg(OH)₂ catalysts are shown in **Fig. 3**. **Fig. 3a** and **b** shows the TEM and HRTEM images of the Au₁/Mg(OH)₂

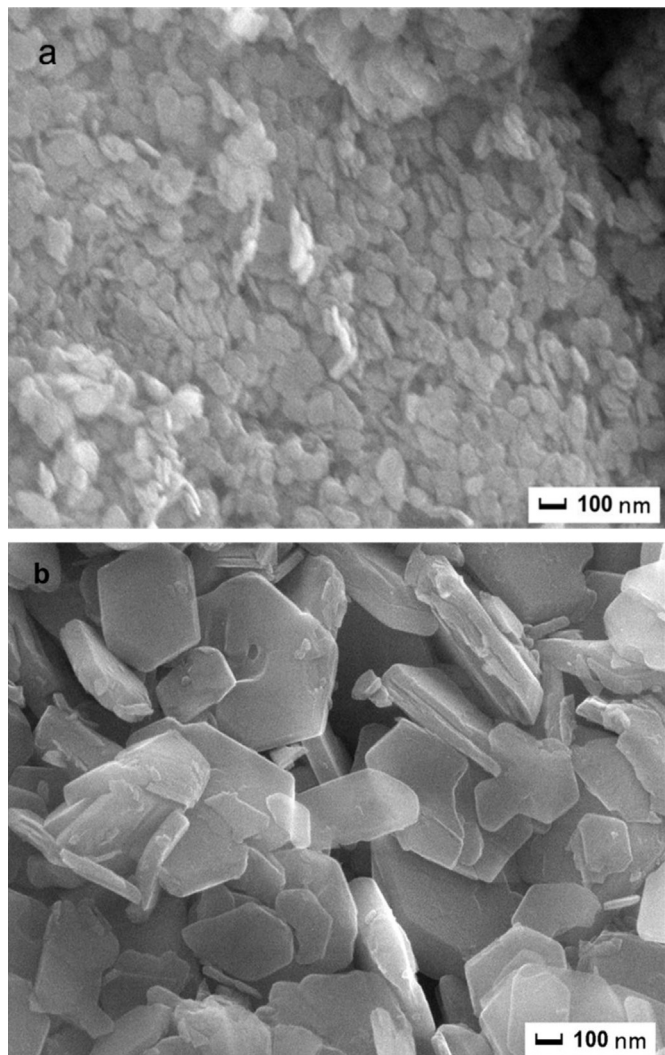


Fig. 2. SEM images of (a) as-prepared Mg(OH)₂ and (b) bulk Mg(OH)₂ samples.

catalyst. The particle sizes of Au nanoparticles in Au₁/Mg(OH)₂ catalyst ranged from 4 to 8 nm and the average particle size was 6 nm. Au nanoparticles with spherical shape were well dispersed on the surfaces of Mg(OH)₂ nanoslices. The HRTEM image (**Fig. 3b**) shows that the lattice fringes of Au nanoparticles were examined to be 0.236 and 0.203 nm, close to the {111} and {200} lattice spacings of fcc metallic gold, respectively. The HRTEM image indicates that the Au nanoparticles had polycrystalline structure.

Fig. 3i and **j** shows the TEM and HRTEM images of Pd₁/Mg(OH)₂ catalyst. It was found that spherical Pd nanoparticles were well dispersed on the surfaces of Mg(OH)₂ nanoslices. The particle sizes of Pd nanoparticles ranged from 2 to 5 nm and the average particle size was 4 nm. The HRTEM image (**Fig. 3j**) shows that the lattice fringes of Pd nanoparticle were examined to be 0.223 nm, close to the {111} lattice spacing of fcc metallic palladium. The HRTEM image indicates that the Pd nanoparticles had single crystalline structure.

Fig. 3c and **d** shows the TEM and HRTEM images of Au_{0.75}Pd_{0.25}/Mg(OH)₂ catalyst. The TEM image shows that the irregular particulates with the average particle size of ca. 13 nm were dispersed on the surfaces of Mg(OH)₂ nanoslices. The HRTEM image (**Fig. 3d**) shows that the irregular particulates were constructed by the coalescence of small-sized Au (5 nm) and Pd (2 nm) nanoparticles. The lattice fringes show that metallic Au and Pd nanoparticles were formed.

Fig. 3e and **f** show the TEM and HRTEM images of $\text{Au}_{0.5}\text{Pd}_{0.5}/\text{Mg}(\text{OH})_2$ catalyst. The TEM images shows that irregular particulates with the average particle size of *ca.* 11 nm were well dispersed on the surfaces of $\text{Mg}(\text{OH})_2$ nanosized slices. The HRTEM image (**Fig. 3f**) shows that the irregular particulates were constructed by the coalescence of small-sized Au (4 nm) and Pd (4 nm) nanoparticles. The lattice fringes show that metallic Au and Pd nanoparticles were formed.

Fig. 3g and **h** shows the TEM and HRTEM images of $\text{Au}_{0.25}\text{Pd}_{0.75}/\text{Mg}(\text{OH})_2$ catalyst. The TEM image shows that

irregular particulates with the average particle size of *ca.* 18 nm were dispersed on the surfaces of $\text{Mg}(\text{OH})_2$ nanoslices. The HRTEM image (**Fig. 3h**) shows that the irregular particulates were constructed by the coalescence of small-sized Au (3 nm) and Pd (5 nm) nanoparticles. The lattice fringes show that metallic Au and Pd nanoparticles were formed.

Fig. 3k and **l** shows the TEM and HRTEM images of $\text{Au}_{1.5}\text{Pd}_{0.5}/\text{Mg}(\text{OH})_2$ catalyst. The TEM image clearly shows that irregular nanoparticles with the average particle size of *ca.* 13 nm were well dispersed on the surfaces of $\text{Mg}(\text{OH})_2$ nanoslices. The

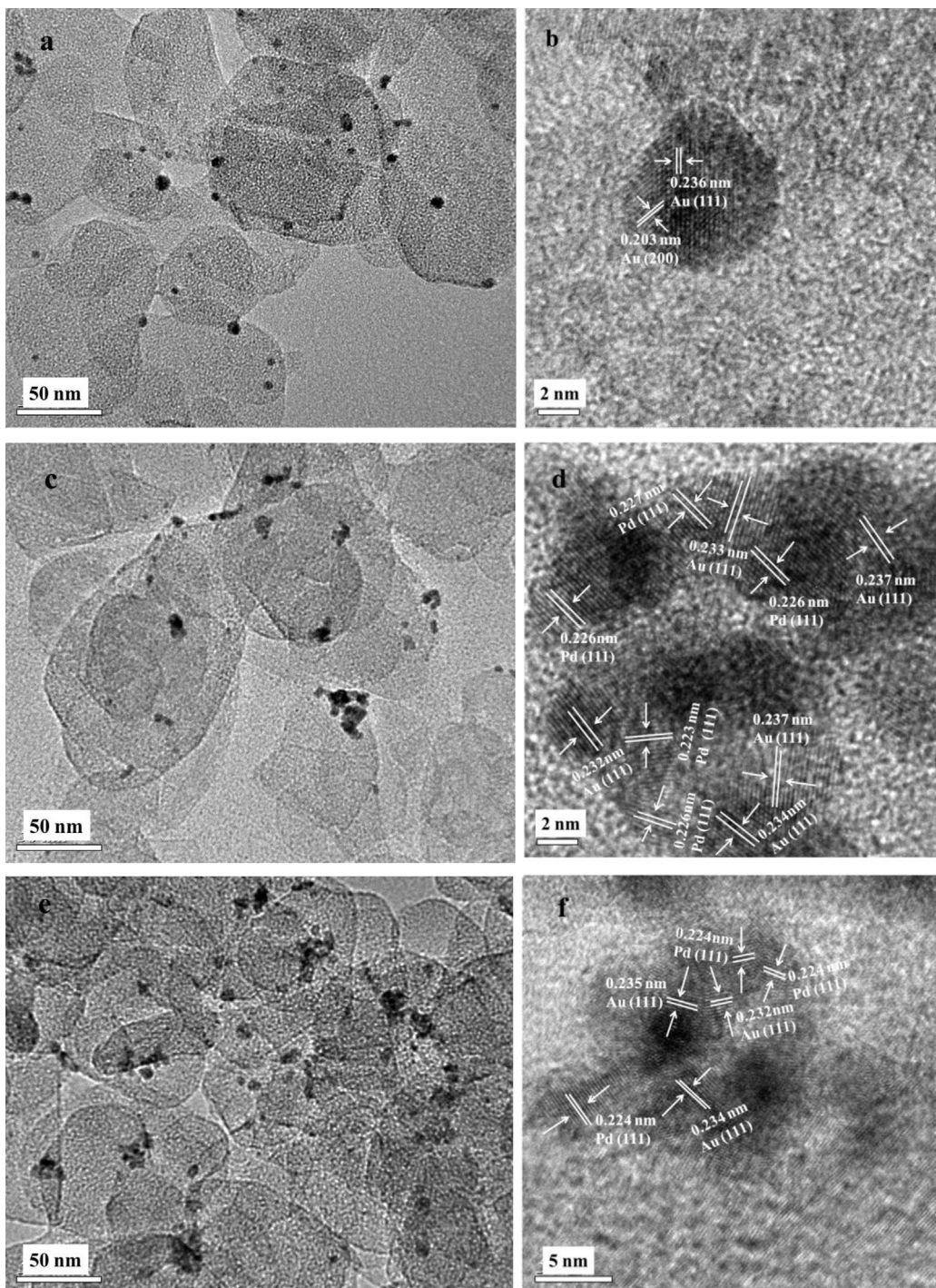
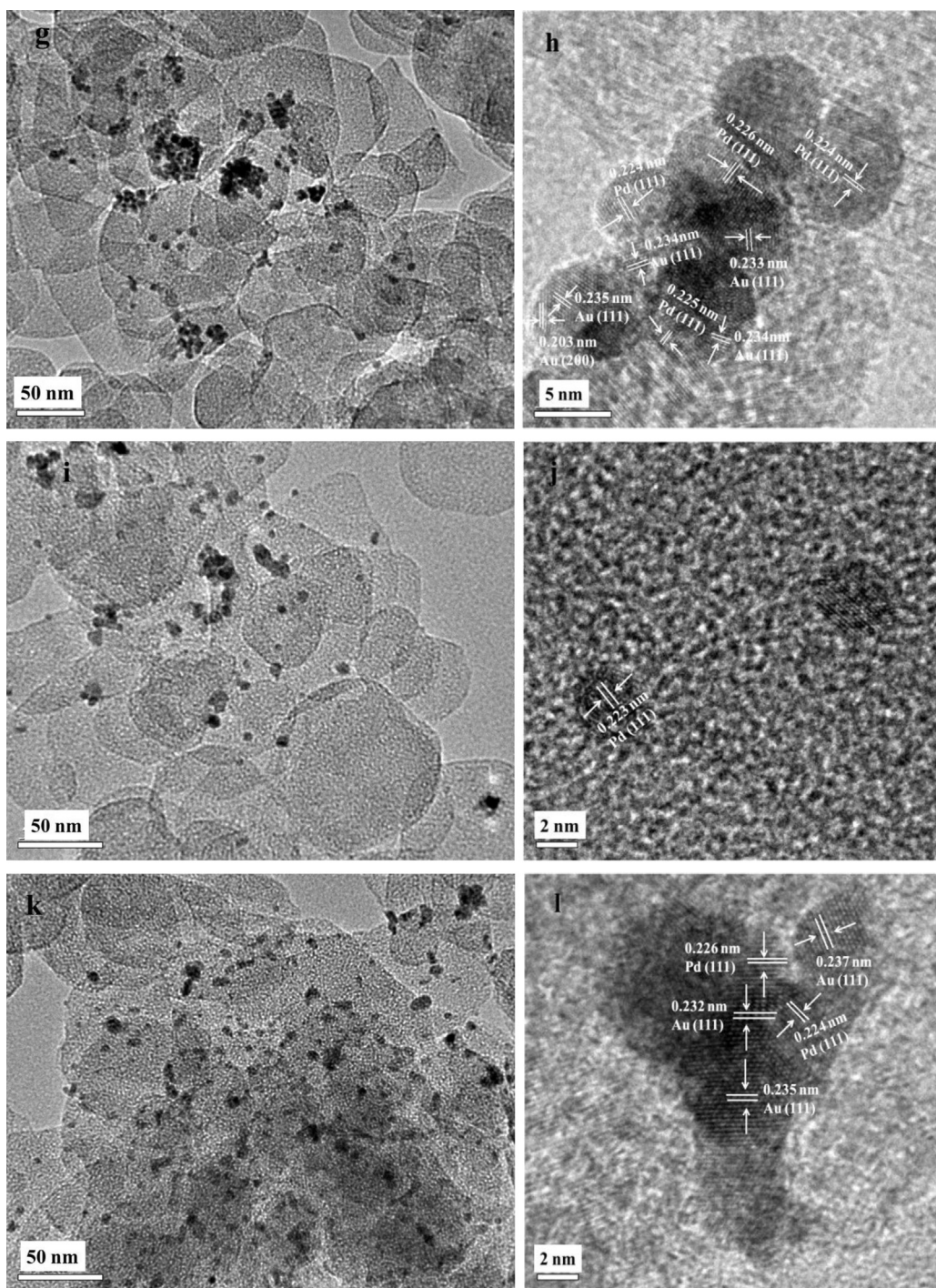


Fig. 3. TEM and HRTEM images of ((a) and (b)) $\text{Au}_1/\text{Mg}(\text{OH})_2$, ((c) and (d)) $\text{Au}_{0.75}\text{Pd}_{0.25}/\text{Mg}(\text{OH})_2$, ((e) and (f)) $\text{Au}_{0.5}\text{Pd}_{0.5}/\text{Mg}(\text{OH})_2$, ((g) and (h)) $\text{Au}_{0.25}\text{Pd}_{0.75}/\text{Mg}(\text{OH})_2$, ((i) and (j)) $\text{Pd}_1/\text{Mg}(\text{OH})_2$, and ((k) and (l)) $\text{Au}_{1.5}\text{Pd}_{0.5}/\text{Mg}(\text{OH})_2$ catalysts.

**Fig. 3.** (Continued)

HRTEM image (Fig. 3l) shows that the irregular nanoparticles were constructed by the coalescence of primary Au (5 nm) and Pd (2 nm) nanoparticles.

The HRTEM images show that the particle number ratio of Au nanoparticles to Pd nanoparticles changed with their contents. The average particle sizes of Au and Pd nanoparticles decreased with decreasing their contents in Au–Pd/Mg(OH)₂ catalysts. Au and Pd nanoparticles coalesced together to form secondary bimetal nanoparticles. The HRTEM analysis certified that there was an interaction between Au and Pd nanoparticles.

3.3. UV-vis DRS analysis

The UV-vis diffusion reflectance spectra of the Au–Pd/Mg(OH)₂ catalysts are shown in Fig. 4. For Au₁/Mg(OH)₂ catalyst, a peak appearing at ca. 530 nm was observed, which is the characteristic surface plasmon resonance of metallic Au nanoparticles [29,30]. In the case of Pd₁/Mg(OH)₂ catalyst, a broad peak ranging from 220 to 900 nm ascribed to the characteristic surface plasmon resonance of metallic Pd nanoparticles was observed. The plasmon bands appearing at ca. 210 nm for all the samples resulted from Mg(OH)₂

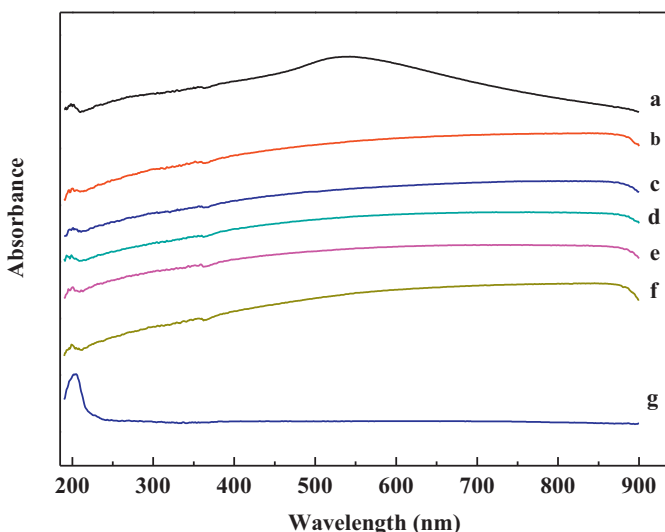


Fig. 4. UV-vis diffuse reflectance spectra of (a) $\text{Au}_1/\text{Mg}(\text{OH})_2$, (b) $\text{Au}_{0.75}\text{Pd}_{0.25}/\text{Mg}(\text{OH})_2$, (c) $\text{Au}_{0.5}\text{Pd}_{0.5}/\text{Mg}(\text{OH})_2$, (d) $\text{Au}_{0.25}\text{Pd}_{0.75}/\text{Mg}(\text{OH})_2$, (e) $\text{Pd}_1/\text{Mg}(\text{OH})_2$, (f) $\text{Au}_{1.5}\text{Pd}_{0.5}/\text{Mg}(\text{OH})_2$, and (g) $\text{Mg}(\text{OH})_2$.

support. For the Au–Pd/Mg(OH)₂ bimetallic catalysts, there were broad peaks ranging from 220 to 900 nm observed. No sharp peak at 530 nm ascribed to metallic Au nanoparticles was observed for all the bimetallic Au–Pd/Mg(OH)₂ catalysts. The UV–vis DRS analysis certified that there was an interaction between Au and Pd nanoparticles, which was consistent with the HRTEM analysis. Furthermore, there were no obvious peaks ascribed to Au^{3+} at $\lambda_{\text{max}} = 220 \text{ nm}$ and Pd^{2+} at $\lambda_{\text{max}} = 238 \text{ nm}$ detected for all the catalysts, indicating that AuCl_4^- and Pd^{2+} were totally reduced to metallic Au and Pd nanoparticles under our present experimental conditions [29].

3.4. O_2 -TPD analysis

Fig. 5 shows the O_2 -TPD profiles of the Mg(OH)₂ support and the Au–Pd/Mg(OH)₂ catalysts. Before absorbing O₂ at room temperature, the catalysts were calcined at 450 °C for 2 h in order to remove the water of catalysts. In this process, Mg(OH)₂ was converted to MgO.

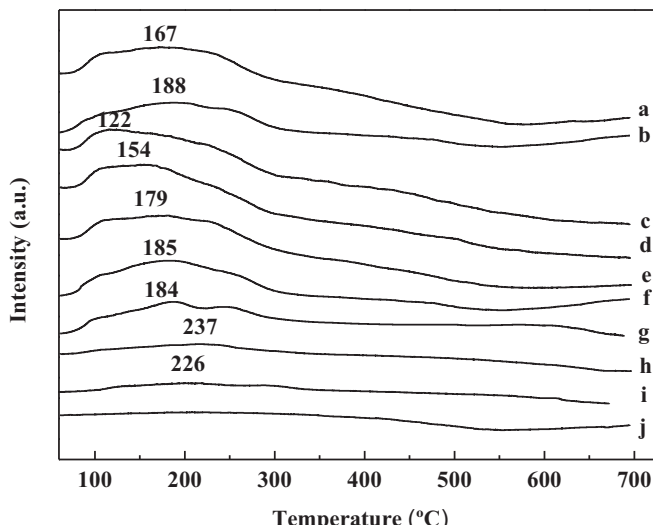


Fig. 5. O_2 -TPD patterns of (a) $\text{Au}_1/\text{Mg}(\text{OH})_2$, (b) $\text{Au}_{0.75}\text{Pd}_{0.25}/\text{Mg}(\text{OH})_2$, (c) $\text{Au}_{0.5}\text{Pd}_{0.5}/\text{Mg}(\text{OH})_2$, (d) $\text{Au}_{0.25}\text{Pd}_{0.75}/\text{Mg}(\text{OH})_2$, (e) $\text{Pd}_1/\text{Mg}(\text{OH})_2$, (f) $\text{Au}_{1.5}\text{Pd}_{0.5}/\text{Mg}(\text{OH})_2$, (g) nanosized $\text{Mg}(\text{OH})_2$, (h) $\text{Au}_{0.75}\text{Pd}_{0.25}/\text{bulk-Mg}(\text{OH})_2$, (i) bulk $\text{Mg}(\text{OH})_2$, and (j) nanosized $\text{Mg}(\text{OH})_2$ without O₂ absorption.

For the Mg(OH)₂ nanoslices, an O₂ desorption peak appearing at 184 °C was observed in the O₂-TPD profile, while no O₂ desorption peak was observed without O₂ absorption treatment, indicating that the resultant MgO support could adsorb O₂. It was reported that in the preparation of MgO, the lattice oxygen was reduced with increasing the calcination temperature [31]. The formation of oxygen defects was probably the reason why high temperature-treated Mg(OH)₂ sample could adsorb O₂. For the Au–Pd/Mg(OH)₂ catalysts, they had the O₂ desorption peaks at the temperatures of 122–188 °C. The O₂ desorption amounts of Au–Pd/Mg(OH)₂ catalysts were larger than that of nanosized Mg(OH)₂ support (Table 1), indicating that Au and Pd nanoparticles adsorbed O₂. The O₂ desorption amounts were in an order of $\text{Au}_{1.5}\text{Pd}_{0.5}/\text{Mg}(\text{OH})_2 > \text{Au}_{0.75}\text{Pd}_{0.25}/\text{Mg}(\text{OH})_2 > \text{Au}_1/\text{Mg}(\text{OH})_2 \approx \text{Pd}_1/\text{Mg}(\text{OH})_2 \approx \text{Au}_{0.5}\text{Pd}_{0.5}/\text{Mg}(\text{OH})_2 \approx \text{Au}_{0.25}\text{Pd}_{0.75}/\text{Mg}(\text{OH})_2 > \text{Mg}(\text{OH})_2$. The O₂ desorption amount obviously increased with the increase in the noble metal content. However, the weight ratio of Au to Pd had little effect on the O₂ desorption amount.

As compared with the as-prepared Mg(OH)₂ nanoslices, the bulk Mg(OH)₂ slices had low O₂ desorption amount. The bulk Mg(OH)₂ slice-supported Au–Pd catalyst, $\text{Au}_{0.75}\text{Pd}_{0.25}/\text{bulk-Mg}(\text{OH})_2$, had lower O₂ desorption amount than the $\text{Au}_{0.75}\text{Pd}_{0.25}/\text{Mg}(\text{OH})_2$ catalyst. The results revealed that nanosized Mg(OH)₂ support endowed the catalysts with high O₂ adsorption ability. Furthermore, it was found that the desorption amount of O₂ ($24.4 \mu\text{mol g}^{-1}$) from the Au and Pd nanoparticles of $\text{Au}_{0.75}\text{Pd}_{0.25}/\text{Mg}(\text{OH})_2$ catalyst was higher than that ($8.3 \mu\text{mol g}^{-1}$) of $\text{Au}_{0.75}\text{Pd}_{0.25}/\text{bulk-Mg}(\text{OH})_2$ catalyst, revealing that the property of Mg(OH)₂ support also affected the O₂ adsorption abilities of Au and Pd nanoparticles.

3.5. Catalytic oxidation of 1,2-propanediol

3.5.1. Effect of Au/Pd ratio

To investigate the effect of Au/Pd ratios on catalytic activity, the catalytic oxidation of 1,2-propanediol was carried out over the Au–Pd/Mg(OH)₂ catalysts with different Au/Pd ratios under 1 MPa of O₂ at 60 °C for 1 h. The results are listed in Table 1. No conversion of 1,2-propanediol was obtained when using Mg(OH)₂ support as the catalyst. However, when the noble metals were supported on Mg(OH)₂ nanoslices, the Au–Pd/Mg(OH)₂ catalysts showed high catalytic activities for the oxidation of 1,2-propanediol. According to the conversions of 1,2-propanediol, the oxidation rates over Au–Pd/Mg(OH)₂ catalysts were in an order of $\text{Au}_{1.5}\text{Pd}_{0.5}/\text{Mg}(\text{OH})_2 \gg \text{Au}_{0.75}\text{Pd}_{0.25}/\text{Mg}(\text{OH})_2 > \text{Au}_{0.5}\text{Pd}_{0.5}/\text{Mg}(\text{OH})_2 > \text{Au}_{0.25}\text{Pd}_{0.75}/\text{Mg}(\text{OH})_2 > \text{Au}_1/\text{Mg}(\text{OH})_2 > \text{Pd}_1/\text{Mg}(\text{OH})_2$. The results showed that the oxidation rates increased with increasing Au contents in the bimetallic catalysts. $\text{Au}_{1.5}\text{Pd}_{0.5}/\text{Mg}(\text{OH})_2$ and $\text{Au}_{0.75}\text{Pd}_{0.25}/\text{Mg}(\text{OH})_2$ catalysts had high catalytic oxidation activities than the others. Interestingly, they also had high O₂ adsorption ability. However, the catalytic oxidation rates over $\text{Au}_{0.5}\text{Pd}_{0.5}/\text{Mg}(\text{OH})_2$ and $\text{Au}_{0.25}\text{Pd}_{0.75}/\text{Mg}(\text{OH})_2$ were obviously higher than those over $\text{Au}_1/\text{Mg}(\text{OH})_2$ and $\text{Pd}_1/\text{Mg}(\text{OH})_2$ catalysts even they had similar O₂ adsorption abilities. Furthermore, the TOF values of bimetallic Au–Pd/Mg(OH)₂ catalysts were higher than those of $\text{Au}_1/\text{Mg}(\text{OH})_2$ and $\text{Pd}_1/\text{Mg}(\text{OH})_2$ catalysts. It was reasonable to conclude that Au and Pd synergistically catalyzed the oxidation reaction.

When the oxidation of 1,2-propanediol was carried out over the Au–Pd/Mg(OH)₂ catalysts with different Au/Pd ratios under the present experimental conditions, the products were lactic acid, acetic acid, and formic acid. Carbon mass was balanced. The selectivities of lactic acid over $\text{Au}_{0.75}\text{Pd}_{0.25}/\text{Mg}(\text{OH})_2$, $\text{Au}_{0.5}\text{Pd}_{0.5}/\text{Mg}(\text{OH})_2$, and $\text{Au}_{0.25}\text{Pd}_{0.75}/\text{Mg}(\text{OH})_2$ were more than 94%, higher than those over $\text{Au}_1/\text{Mg}(\text{OH})_2$ (79.2%), $\text{Pd}_1/\text{Mg}(\text{OH})_2$ (92.6%), and $\text{Au}_{1.5}\text{Pd}_{0.5}/\text{Mg}(\text{OH})_2$ (83.8%) catalysts. For the

Au–Pd/Mg(OH)₂ catalysts, both formic and acetic acids were formed as by products. The total selectivities of both formic and acetic acids over Au_{0.75}Pd_{0.25}/Mg(OH)₂, Au_{0.5}Pd_{0.5}/Mg(OH)₂, and Au_{0.25}Pd_{0.75}/Mg(OH)₂ were less than 6%. The results revealed that in a wide range of Au/Pd ratios, the Au–Pd/Mg(OH)₂ catalysts gave high catalytic activities for the catalytic oxidation of 1,2-propanediol to lactic acid. Au and Pd nanoparticles on Mg(OH)₂ support synergistically catalyzed the selective oxidation of 1,2-propanediol to lactic acid.

The catalytic activity of bulk Mg(OH)₂-supported Au and Pd nanoparticles catalyst in the oxidation of 1,2-propanediol was also investigated. The conversion of 1,2-propanediol and the selectivity of lactic acid over Au_{0.75}Pd_{0.25}/bulk-Mg(OH)₂ catalyst were less than those over Au_{0.75}Pd_{0.25}/Mg(OH)₂ catalyst, respectively. Small-sized Mg(OH)₂ support endowed Au and Pd nanoparticles with high catalytic activity in the oxidation of 1,2-propanediol to lactic acid.

Considering Au_{0.75}Pd_{0.25}/Mg(OH)₂ catalyst gave high catalytic activity in the oxidation of 1,2-propanediol to lactic acid, it was selected as the model catalyst in the following experiments.

3.5.2. Effect of reaction temperature

Fig. 6a shows the conversions of 1,2-propanediol and the selectivities of lactic acid in the oxidation of 1,2-propanediol catalyzed by Au_{0.75}Pd_{0.25}/Mg(OH)₂ catalyst at different reaction temperatures. When the reaction times were 60 and 240 min, respectively, the conversions of 1,2-propanediol increased from 7.6% to 60.9% and from 30.5% to 97.5% with increasing the reaction temperatures from 30 to 60 °C (**Fig. 6a1**) while the selectivities of lactic acid decreased from 97.8% to 94% and from 95.6% to 88% (**Fig. 6a2**). The results indicated that the conversion of 1,2-propanediol increased while the selectivity of lactic acid decreased with increasing the reaction temperature. The selectivities of acetic acid and formic acid were less than 7.4% and 4.6%, respectively, after reacting at 60 °C for 240 min (see Fig. S1). The selectivities of acetic acid and formic acid slightly increased with increasing the reaction temperature and prolonging the reaction time.

3.5.3. Effect of NaOH concentration

When the mole ratios of NaOH to 1,2-propanediol were 1:1, 2:1, and 3:1, the conversions of 1,2-propanediol gradually increased from 18.6% to 90.6%, 26.1% to 97.5% and 26.4% to 98.2% while the selectivities of lactic acid decreased from 88.6% to 83.1%, 95.0% to 88% and 96.5% to 90%, respectively, with increasing the reaction times from 30 to 240 min (**Fig. 6b**). At the low mole ratio of NaOH to 1,2-propanediol of 1:1, the selectivities of formic acid increased from 9.1% to 12.6% with increasing the reaction times from 30 to 240 min (see Fig. S1). When the mole ratios of NaOH to 1,2-propanediol were increased to 2:1 and 3:1, the selectivities of formic acid were less than 4.8%. The selectivities of acetic acid were less than 4.3% when the oxidation reaction was carried out with different mole ratios of NaOH to 1,2-propanediol (see Fig. S1). The results showed that high NaOH concentration was favorable to the selective oxidation of 1,2-propanediol to lactic acid over Au_{0.75}Pd_{0.25}/Mg(OH)₂ catalyst.

3.5.4. Effect of 1,2-propanediol concentration

Fig. 6c shows the conversions of 1,2-propanediol and the selectivities of lactic acid in the catalytic oxidation of 1,2-propanediol over Au_{0.75}Pd_{0.25}/Mg(OH)₂ catalyst under different 1,2-propanediol concentrations. When the concentrations of 1,2-propanediol were 0.13, 0.26, 0.52, and 0.78 mol L⁻¹, the conversions of 1,2-propanediol were 100%, 97.5%, 93.9%, and 89.0%, respectively, after reacting at 60 °C for 240 min. The selectivities of lactic acid were 86.7%, 88.0%, 92.0%, and 95.5%. The selectivities of formic acid and acetic acid were less than 8.5% and 4.8%, respectively (see Fig. S1). The conversions of 1,2-propanediol increased with

decreasing the concentration of 1,2-propanediol and prolonging the reaction time. The selectivities of lactic acid decreased while the selectivities of acetic and formic acids increased with decreasing the concentration of 1,2-propanediol and prolonging the reaction time. It can be explained as that under low 1,2-propanediol concentration, more catalytic active sites are available on the surface of the Au_{0.75}Pd_{0.25}/Mg(OH)₂ catalyst, leading to the cleavage and oxidation of resultant lactic acid or intermediates to form more formic and acetic acids.

3.5.5. Effect of O₂ pressure

Fig. 6d shows the conversions of 1,2-propanediol and the selectivities of lactic acid in the catalytic oxidation of 1,2-propanediol over Au_{0.75}Pd_{0.25}/Mg(OH)₂ catalyst under different O₂ pressures. After reacting at 60 °C for 240 min, the conversions of 1,2-propanediol were 24.7%, 60.3%, 97.5%, and 99.0% at the O₂ pressures of 0.3, 0.6, 1.0, and 1.3 MPa, respectively. The selectivities of lactic acid were 91.2%, 90%, 88%, and 87.7%. The selectivities of formic acid and acetic acid were less than 7.6% and 4.8%, respectively (see Fig. S1). The conversions of 1,2-propanediol increased while the selectivities of lactic acid decreased with raising the O₂ pressure and prolonging the reaction time.

3.5.6. Effect of catalyst loading

Fig. 6e shows the conversions of 1,2-propanediol and the selectivities of lactic acid in the oxidation of 1,2-propanediol with different catalyst loadings. After reacting at 60 °C for 120 min, the conversions of 1,2-propanediol were 54.9%, 91.4%, 96.3%, and 99.3% when the catalyst loadings were 0.2, 0.4, 0.6, and 0.8 g, respectively. The selectivities of lactic acid were 92.8%, 92.7%, 82.1%, and 75%. The conversion of 1,2-propanediol increased while the selectivity of lactic acid decreased with increasing catalyst loading and prolonging the reaction time. With high catalyst loadings of 0.6 and 0.8 g, the selectivities of formic acid and acetic acid reached 10.3% and 16.0%; 7.7% and 9.0%, respectively (see Fig. S1), at the complete conversion of 1,2-propanediol. Increasing catalyst loading caused the oxidation of lactic acid and intermediates to form more formic and acetic acids.

3.6. Reaction kinetics

3.6.1. Preliminary considerations

A power-function type reaction kinetic equation was used to investigate the effect of reaction parameters, such as, reaction temperature, 1,2-propanediol concentration, O₂ pressure, catalyst loading, on the reaction rate. Although NaOH concentration had obvious effect on the reaction rate, the effect of NaOH concentration on the reaction rate was ignored herein because the mole ratio of NaOH to 1,2-propanediol was fixed at 2:1 in our present experiments for modeling the reaction kinetics. On the other hand, side reactions for the formation of formic acid and acetic acid were ignored because the initial reaction rates were used to fit the reaction kinetics and the amounts of formic acid and acetic acid were very small at initial reaction step. Au_{0.75}Pd_{0.25}/Mg(OH)₂ was used as the catalyst in the reaction kinetic modeling due to that it showed high catalytic activity toward the oxidation of 1,2-propanediol to lactic acid.

The power-function type reaction kinetic equation is expressed as follows.

$$r = -\frac{dC_p}{dt} = k C_p^a P_{O_2}^b W_{cat}^c \quad (1)$$

where *k* is the rate constant. *a*, *b*, and *c* are the reaction orders with respect to the concentration of 1,2-propanediol, O₂ pressure, and weight of catalyst. *r* is the initial reaction rate of 1,2-propanediol, mol L⁻¹ min⁻¹. *C_p* is the initial concentration of 1,2-propanediol,

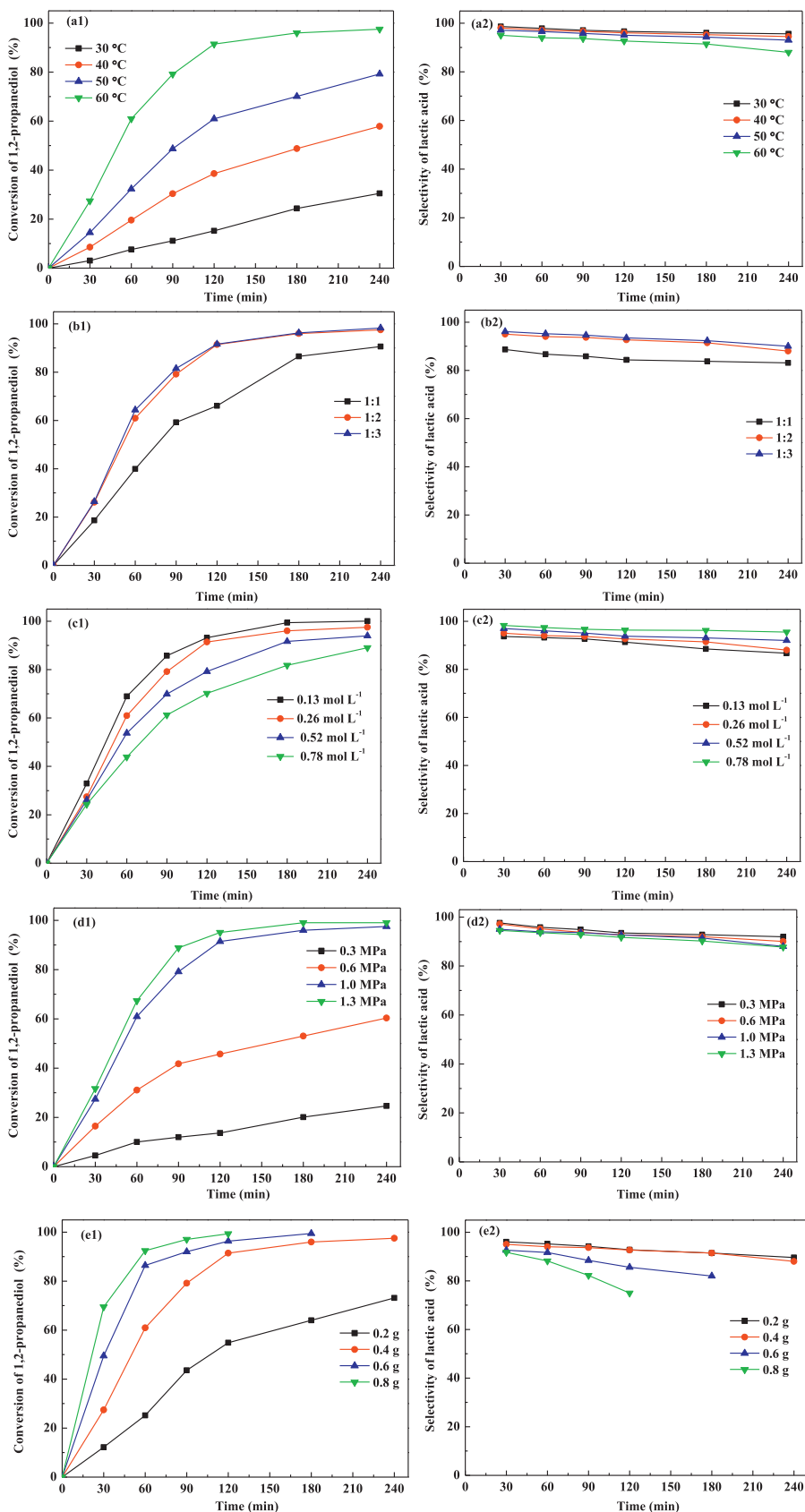


Fig. 6. Conversions of 1,2-propanediol and selectivities of lactic acid in the catalytic oxidation of 1,2-propanediol with O₂ over Au_{0.75}Pd_{0.25}/Mg(OH)₂ catalyst under different reaction conditions. The stirring rate was fixed at 700 rpm. (a) Catalyst, 0.4 g; O₂, 1.0 MPa; NaOH, 0.52 mol L⁻¹; 1,2-propanediol aqueous solution, 0.26 mol L⁻¹, 200 mL; reaction temperatures, 30, 40, 50, and 60 °C. (b) Catalyst, 0.4 g; O₂, 1.0 MPa; mole ratios of NaOH to 1,2-propanediol of 1:1, 2:1, and 3:1; 1,2-propanediol aqueous solution, 0.26 mol L⁻¹, 200 mL; reaction temperature, 60 °C. (c) Catalyst, 0.4 g; O₂, 1.0 MPa; NaOH, 0.52 mol L⁻¹; 1,2-propanediol aqueous solution, 0.13, 0.26, 0.52, and 0.78 mol L⁻¹, 200 mL, reaction temperature, 60 °C. (d) Catalyst, 0.4 g; O₂, 0.3, 0.6, 1.0, and 1.3 MPa; NaOH, 0.52 mol L⁻¹; 1,2-propanediol aqueous solution, 0.26 mol L⁻¹, 200 mL; reaction temperature, 60 °C. (e) Catalyst, 0.2, 0.4, 0.6, and 0.8 g; O₂, 1.0 MPa; NaOH, 0.52 mol L⁻¹; 1,2-propanediol aqueous solution, 0.26 mol L⁻¹, 200 mL; reaction temperature, 60 °C.

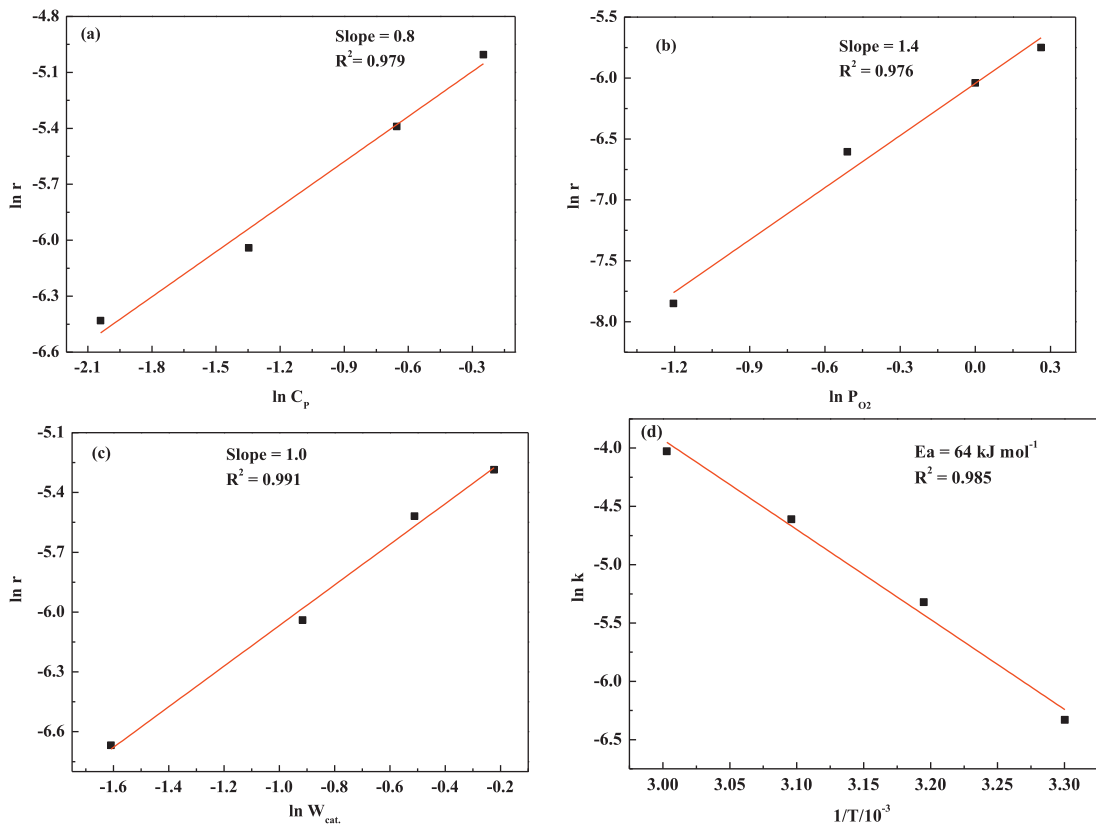


Fig. 7. Estimation of the reaction orders and the reaction activation energy for the power-function type reaction kinetics.

mol L⁻¹. P_{O_2} is the initial O₂ pressure, MPa. W_{cat} is the catalyst weight, g. The rate constant k follows the Arrhenius equation.

$$k = A \exp\left(-\frac{E_a}{RT}\right) \quad (2)$$

where A is the pre-exponential factor and E_a is the activation energy, kJ mol⁻¹. R is the ideal gas constant, 8.314×10^{-3} kJ mol⁻¹ K⁻¹. T is the reaction temperature, K.

3.6.2. Diffusion effect

Considering that the Au_{0.75}Pd_{0.25}/Mg(OH)₂ catalyst was prepared by the sol-immobilization of Au and Pd nanoparticles on the surfaces of Mg(OH)₂ nanoslices, the effect of mass diffusion on the reaction rate should be mainly caused by the external diffusion. In order to eliminate the external diffusion, the catalytic oxidation of 1,2-propanediol was tested at different stirring speeds (see Fig. S2).

As shown in Fig. S2, when the stirring speeds were increased to 700 and 800 rpm, the conversions of 1,2-propanediol were overlapped at different reaction times. The results showed that the external diffusion was completely eliminated at the stirring speed of 700 rpm.

3.6.3. Reaction orders

A linear Eq. (3) is obtained by taking the natural logarithm of both sides of Eq. (1).

$$\ln r = \ln \left(-\frac{dC_p}{dt} \right) = \ln k + a \ln C_p + b \ln P_{O_2} + c \ln W_{cat} \quad (3)$$

To calculate the reaction orders of a , b , and c according to Eq. (3), the initial rates were calculated according to the data shown in Fig. 6c–e. The initial reaction rates of 1,2-propanediol under different reaction conditions were calculated in the first 30 min.

Fig. 7a shows the line by plotting ln r vs ln C_p. The data used in Fig. 7a were calculated according to those shown in Fig. 6c1. A

straight line was obtained while plotting ln r vs ln C_p. The straight line gave good linear correlation of 0.979. The reaction order of 1,2-propanediol, a , is 0.8 according to the slope of the straight line.

Fig. 7b shows the line by plotting ln r vs ln P_{O₂}. The data used in Fig. 7b were calculated according to those shown in Fig. 6d1. A straight line was obtained while plotting ln r vs ln P_{O₂}. The straight line gave good linear correlation of 0.976. The reaction order of O₂, b , is 1.4 according to the slope of the straight line.

Fig. 7c shows the line by plotting ln r vs ln W_{cat}. The data used in Fig. 7c were calculated according to those shown in Fig. 6e1. A straight line was obtained while plotting ln r vs ln W_{cat}. The straight line gave good linear correlation of 0.991. The reaction order of W_{cat}, c , is 1.0 according to the slope of the straight line.

The power-function type reaction kinetic equation can be written as follows.

$$r = -\frac{dC_p}{dt} = k C_p^{0.8} P_{O_2}^{1.4} W_{cat}^{1.0} \quad (4)$$

3.6.4. Activation energy

According to the data shown in Fig. 6a1, the value of reaction rate constant, k , can be calculated by using Eq. (4). The values of k are 0.00178, 0.004884, 0.009948, and 0.017801 at the reaction temperatures of 30, 40, 50, and 60 °C, respectively.

Eq. (2) can be rearranged as follows.

$$\ln k = \ln A - \left(\frac{E_a}{R} \right) \left(\frac{1}{T} \right) \quad (5)$$

A straight line with a good linear correlation of 0.985 was obtained while plotting ln k vs 1/T (Fig. 7d). The reaction activation energy, E_a , is 64 kJ mol⁻¹ according to the slope of the straight line.

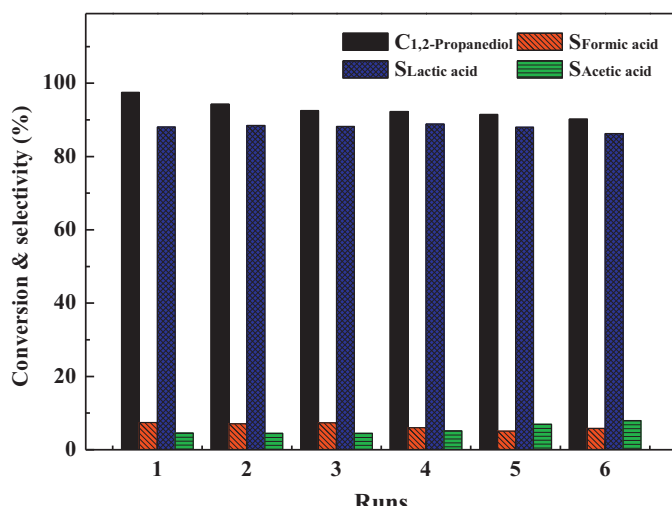


Fig. 8. Recycling performance of Au_{0.75}Pd_{0.25}/Mg(OH)₂ catalyst in the oxidation of 1,2-propanediol. Reaction conditions: reaction temperature, 60 °C; reaction time, 240 min; 1,2-propanediol solution, 200 mL, 0.26 mol L⁻¹; O₂, 1.0 MPa; catalyst, 0.4 g; NaOH, 0.52 mol L⁻¹; stirring rate, 700 rpm.

3.7. Catalyst recycling and comparison with previous works

The recycling performance of Au_{0.75}Pd_{0.25}/Mg(OH)₂ catalyst in the oxidation of 1,2-propanediol is shown in Fig. 8. After reacting at 60 °C for 240 min, the used catalyst was filtrated and dried at 120 °C for 12 h before next recycling. As shown in Fig. 8, the conversion of 1,2-propanediol and the selectivity of lactic acid over the fresh Au_{0.75}Pd_{0.25}/Mg(OH)₂ catalyst were 97.5% and 88%, respectively. After recycling for 6 times, the conversion of 1,2-propanediol and the selectivity of lactic acid over the recycled Au_{0.75}Pd_{0.25}/Mg(OH)₂ catalyst were 90.2% and 86.2%, respectively. The results showed that the Au_{0.75}Pd_{0.25}/Mg(OH)₂ catalyst had good recycling performance. After recycling for 6 times, the weight percentages of Au and Pd in the spent Au_{0.75}Pd_{0.25}/Mg(OH)₂ catalyst were 0.71% and 0.2%, respectively, indicating that only small amounts of Au and Pd nanoparticles were leached during the reaction as compared to those in the fresh catalyst.

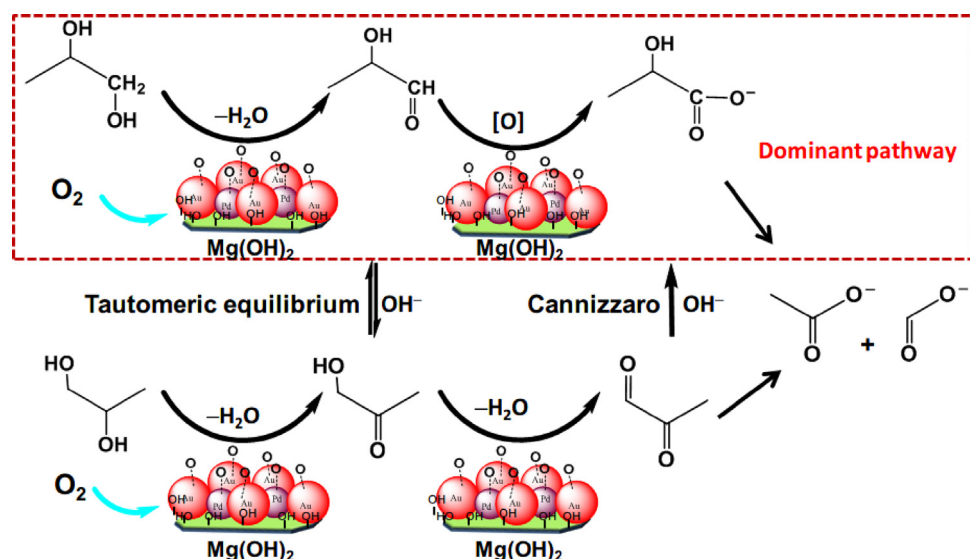
Several literatures [17,21–23,32] have reported the oxidation of 1,2-propanediol to lactic acid catalyzed by supported noble

monometallic or bimetallic catalysts, such as 2.8%Au/MgO [21], 1%AuPt/C [22], 0.75%Pt–0.25%Au/C [23], 0.45%Au–5%Pd/C [32], 1%AuPd/C_{SiM} [17], and 1%AuPd/TiO₂_{SiM} [17]. The catalytic performances are listed in Table S2. These catalysts showed high catalytic activities for the selective oxidation of 1,2-propanediol to lactic acid with the selectivity of more than 90% under different reaction conditions, but had different TOFs. The TOFs of these catalysts were in an order of 2.8%Au/MgO (111) < 1%AuPt/C (380) < 0.75%Pt–0.25%Au/C (475) < 0.45%Au–5%Pd/C (760) < 1%AuPd/C_{SiM} (1066) < 1%AuPd/TiO₂_{SiM} (1880). Au–Pd/Mg(OH)₂ catalysts reported in this work had TOFs ranging from 1347 to 1776 and their lactic acid selectivities were more than 83.8%, indicating that Au–Pd/Mg(OH)₂ catalysts are effective for the catalytic oxidation of 1,2-propanediol to lactic acid.

3.8. Reaction mechanism

In the catalytic oxidation of 1,2-propanediol, the reactions may involve the oxidation of terminal and middle hydroxyl groups of 1,2-propanediol as shown in Scheme 1. If the oxidation of the terminal hydroxyl group occurs, 1,2-propanediol can be oxidized to lactaldehyde. The resultant lactaldehyde can be rapidly oxidized to lactic acid because the intermediate, lactaldehyde, is not detected under our present experimental conditions. If the oxidation of middle hydroxyl group occurs, 1,2-propanediol can be oxidized to hydroxyacetone. The resultant hydroxyacetone can be oxidized to pyruvaldehyde, which can be further oxidized to acetic acid and formic acid [17]. Meanwhile, hydroxyacetone can be transformed to lactaldehyde via the tautomeric equilibrium. Then the resultant lactaldehyde is oxidized to lactic acid. Pyruvaldehyde can be converted to lactate in an alkaline solution (Cannizzaro reaction).

To certify the reaction mechanism, controlled experiments were also carried out (the results are listed in Table S1). When the catalytic oxidation of hydroxyacetone was carried out at 60 °C for 30 min in an alkaline solution, the selectivity of lactic acid was only 52.7% at the hydroxyacetone conversion of 97.2%, accompanied with the formation of formic acid and acetic acid. However, when the oxidation of 1,2-propanediol was catalyzed by the Au_{0.75}Pd_{0.25}/Mg(OH)₂ catalyst in an alkaline solution at 60 °C for 240 min (see Fig. 6a), the selectivity of lactic acid was 88% at the 1,2-propanediol conversion of 97.5%. Furthermore, no hydroxyacetone and pyruvaldehyde were detected in all the present catalysis experiments. The results indicated that the catalytic oxidation of



Scheme 1. Reaction routes in the oxidation of 1,2-propanediol to lactic acid catalyzed by Au_{0.75}Pd_{0.25}/Mg(OH)₂ catalyst.

1,2-propanediol to lactic acid was probably through the terminal hydroxyl group oxidation route.

4. Conclusions

Au and Pd nanoparticles with the particle sizes of 4–8 nm and 2–5 nm were present in bimetallic Au–Pd/Mg(OH)₂ catalysts. The O₂ adsorption ability increased with the increase in the content of noble metals. High noble metal content endowed the Au–Pd/Mg(OH)₂ catalyst with high oxidation activity. The Au and Pd nanoparticles in the Au–Pd/Mg(OH)₂ catalysts synergistically catalyzed the selective oxidation of 1,2-propanediol to lactic acid. When the catalytic oxidation of 1,2-propanediol with O₂ was carried out over Au_{0.75}Pd_{0.25}/Mg(OH)₂ catalyst at 60 °C for 240 min in an alkaline solution, the selectivity of lactic acid was 88% at the 1,2-propanediol conversion of 97.5%. Au_{0.75}Pd_{0.25}/Mg(OH)₂ catalyst had good recycling performance. A power-function type reaction kinetic model well fitted the experimental data, $r = -dC_P/dt = kC_P^{0.8}P_{O_2}^{1.4}W_{cat}^{1.0}$. The reaction activation energy was 64 kJ mol⁻¹.

Acknowledgments

The authors sincerely thank Professor K. Chen (Jiangsu University) for supporting the TEM and HRTEM measurements. This work was financially supported by research funds from Jiangsu Province Education Bureau (11KJB530002, 1102120C and CXZZ12-0683), Jiangsu University for Young Researchers (Nos. 11JDG028 and 2010-4849), China Postdoctoral Foundation Committee (2011M500866), and Ph.D. Innovation Program of Jiangsu Province (CXZZ13-0666).

Appendix A. Supplementary data

Supplementary data associated with this article can be found, in the online version, at <http://dx.doi.org/10.1016/j.apcata.2014.05.022>.

References

- [1] J.P.M. Sanders, J.H. Clark, G.J. Harmsen, H.J. Heeres, J.J. Heijnen, S.R.A. Kersten, W.P.M. van Swaaij, J.A. Moulijn, *Chem. Eng. Process.* 51 (2012) 117–136.

- [2] Y.H. Feng, H.B. Yin, L.Q. Shen, A.L. Wang, Y.T. Shen, T.S. Jiang, *Chem. Eng. Technol.* 36 (2013) 73–82.
- [3] Y.H. Feng, H.B. Yin, A.L. Wang, L.Q. Shen, L.B. Yu, T.S. Jiang, *Chem. Eng. J.* 168 (2011) 403–412.
- [4] S. Hirasawa, H. Watanabe, T. Kizuka, Y. Nakagawa, K. Tomishige, *J. Catal.* 300 (2013) 205–216.
- [5] W.B. Hu, B. Lowry, A. Varma, *Appl. Catal., B: Environ.* 106 (2011) 123–132.
- [6] S. Gilá, M. Marchena, L. Sánchez-Silva, A. Romero, P. Sánchez, J.L. Valverde, *Chem. Eng. J.* 178 (2011) 423–435.
- [7] L.Q. Shen, Y.H. Feng, H.B. Yin, *J. Ind. Eng. Chem.* 17 (2011) 484–492.
- [8] L.Q. Shen, H.B. Yin, A.L. Wang, Y.H. Feng, *Chem. Eng. J.* 180 (2012) 277–283.
- [9] X.Y. Liao, Y.L. Zhu, S.G. Wang, Y.W. Li, *Fuel Process. Technol.* 90 (2009) 988–993.
- [10] S. Bancquart, C. Vanhove, Y. Pouilloux, J. Barrault, *Appl. Catal., A: Gen.* 218 (2001) 1–11.
- [11] A. Corma, S. Iborra, A. Velty, *Chem. Rev.* 107 (2007) 2411–2502.
- [12] J.J. Bozell, G.R. Petersen, *Green Chem.* 12 (2010) 539–554.
- [13] R. Datta, M. Henry, *J. Chem. Technol. Biotechnol.* 81 (2006) 1119–1129.
- [14] W. Timbuntam, K. Sriroth, Y. Tokiwa, *Biotechnol. Lett.* 28 (2006) 811–814.
- [15] I. Ohara, K. Hiyama, T. Yoshida, *Appl. Microbiol. Biotechnol.* 37 (1992) 544.
- [16] J. Sikder, S. Chakraborty, P. Pala, E. Driolic, C. Bhattacharjee, *Biochem. Eng. J.* 69 (2012) 130–137.
- [17] N. Dimitratos, J.A. Lopez-Sánchez, S. Meenakshisundaram, J.M. Anthonykutty, G. Brett, A.F. Carley, S.H. Taylor, D.W. Knight, G.J. Hutchings, *Green Chem.* 11 (2009) 1209–1216.
- [18] C.A. Ramírez-López, J.R. Ochoa-Gómez, M. Fernández-Santos, O. Gómez-Jiménez-Aberasturi, A. Alonso-Vicario, J. Torrecilla-Soria, *Ind. Eng. Chem. Res.* 49 (2010) 6270–6278.
- [19] M. Checa, F. Auneau, J. Hidalgo-Carrillo, A. Marinasa, J.M. Marinas, Catherine Pinel, F.J. Urbano, *Catal. Today* 196 (2012) 91–100.
- [20] R.K.P. Purushothaman, J. van Haveren, D.S. van Es, I. Melián-Cabrera, J.D. Meeldijk, H.J. Heeres, *Appl. Catal., B: Environ.* 147 (2014) 92–100.
- [21] H. Ma, X. Nie, J.Y. Cai, C. Chen, J. Gao, H. Miao, J. Xu, *Sci. China Chem.* 53 (2010) 1497–1501.
- [22] Y. Ryabenkova, Q. He, P.J. Miedziak, N.F. Dummer, S.H. Taylor, A.F. Carley, D.J. Morgan, N. Dimitratos, D.J. Willock, D. Bethell, D.W. Knight, G.J. Hutchings, *Top. Catal.* 55 (2012) 1283–1288.
- [23] D.W. Knight, D. Chadwick, C.J. Kiely, G.J. Hutchings, *Catal. Today* 203 (2013) 139–145.
- [24] H.H.M. Pinxt, B.F.M. Kuster, G.B. Marin, *Appl. Catal., A: Gen.* 191 (2000) 45–54.
- [25] T. Tsujino, T. Ohigashi, S. Sugiyama, K. Kawashiro, H. Hayashi, *J. Mol. Catal.* 71 (1992) 25–35.
- [26] W. Su, Z.Y. Chang, K.L. Gao, D.Z. Wei, *Tetrahedron: Asymmetry* 15 (2004) 1275–1277.
- [27] M.M. Dimos, G.J. Blanchard, *J. Electroanal. Chem.* 654 (2011) 13–19.
- [28] S. Garrettin, P. McMorn, P. Johnston, K. Griffin, G.J. Hutchings, *Chem. Commun.* 7 (2002) 696–697.
- [29] N. Dimitratos, J.A. Lopez-Sánchez, D. Lennon, F. Porta, L. Prati, *Catal. Lett.* 108 (2006) 147–153.
- [30] J.L. Margitfalvi, A. Fási, M. Hegedüs, F. Lónyi, S. Gbils, N. Bogdan-chikova, *Catal. Today* 72 (2002) 157–169.
- [31] J. Puriwat, W. Chaitree, K. Suriye, S. Dokjampa, P. Praserthdam, J. Panpranot, *Catal. Commun.* 12 (2010) 80–85.
- [32] M.B. Griffin, A.A. Rodriguez, M.M. Montemore, J.R. Monnier, C.T. Williams, J.W. Medlin, *J. Catal.* 307 (2013) 111–120.